Hydrogen passivation of shallow donors S, Se, and Te in GaAs

J. Vetterhöffer and J. Weber
Max-Planck-Institut für Festkörperforschung, Postfach 80 06 65, D-70506 Stuttgart, Germany
(Received 12 December 1995; revised manuscript received 20 February 1996)

The passivation by hydrogen of the shallow donors sulfur, selenium, and tellurium in GaAs was studied by infrared absorption spectroscopy, capacitance-voltage (C-V) depth profiling, and secondary-ion-mass spectroscopy (SIMS). The microscopic structure of the hydrogen complexes was identified. The hydrogen atom is bound in the antibonding position to one of the donor's neighboring gallium atoms. The infrared active complex was identified as the passivating hydrogen complex. The dissociation energy of the S-H complexes was determined as $E_{SH}=1.55\pm0.06$ eV with an attempt frequency $\nu_{SH}\sim 2\times10^{13}\,s^{-1}$. [S0163-1829(96)06220-0]

I. INTRODUCTION

Hydrogen incorporation into semiconductors has been shown to be a very common process that occurs both during growth and during post-growth processing such as plasma etching, wet chemical etching, or surface cleaning. These treatments can lead to a hydrogen diffusion up to several micrometers into the material. In recent years, the interaction of hydrogen with impurities in a variety of semiconductors was studied (Si,[1] GaAs,[2] InP,[3] GaP,[4] etc.). It has been shown that hydrogen can electrically passivate both shallow dopants as well as deep defects. Shallow dopant passivation leads to a decrease of the free-carrier concentration of more than one order of magnitude. This effect was explained by a neutralization of the donor ions by the formation of dopant-hydrogen complexes rather than a compensation effect, since passivation leads also to an increase of the Hall mobility.[5,6] Microscopic details of the hydrogen complexes can be obtained by infrared absorption spectroscopy. Vibrational excitation of the hydrogen atom [local vibrational modes (LVM's)] leads to very narrow absorption lines with frequencies very similar to those known for hydrogen containing molecules. In the case of GaAs it is observed that all shallow dopants (C_{As}, Si_{As}, Ge_{As}, Be_{Ga}, Zn_{Ga}, Cd_{Ga}, Si_{Ga}, Sn_{Ga}, S_{As}, Se_{As}, and Te_{As}) are passivated by atomic hydrogen and for most of them vibrational lines were reported.[7]

In contrast to the structure of hydrogen-dopant complexes, the kinetics of hydrogen diffusion in semiconductors and its possible charge states is much less understood. This is due to the variety of trapping and detrapping mechanisms of the hydrogen atom during its motion. Drift experiments in the electric field of a GaAs Schottky diode have shown that, depending on the Fermi level, hydrogen can exist at least in a positive[8] and in a negative charge state.[9] Numeric modeling of deuterium diffusion experiments estimates the hydrogen acceptor level in GaAs at 0.1 ± 0.05 eV below the conduction band[10] and the donor level at 1.1 ± 0.05 eV below the conduction band.[11] By monitoring the occurrence of carbon-hydrogen complexes as a function of Fermi level, Clerjaud *et al.*[12] located the donor level at 0.5 ± 0.1 eV above the valence band. Finally, Roos *et al.*[13] give an *upper* limit for the acceptor level at ~0.12 eV below the conduction band. This suggests that hydrogen in GaAs can be present in three charge states H^+, H^0, and H^- depending on the Fermi level position (positive-U case). In contrast, from first-principles calculations, Pavesi and Giannozzi propose the inverse ordering, where the neutral charge state H^0 is not stable (negative-U case).[14]

Concerning the complexing of hydrogen with the group-VI shallow donors S, Se, and Te, only little is known. In an early work, Pearton *et al.*[15] reported a 100% passivation of the implanted species after hydrogen plasma exposure and a complete reactivation after annealing above 350 °C. The dissociation energy of the Se-H complexes was determined by Leitch, Prescha, and Weber.[9] The increasing electron mobility after hydrogen passivation was shown by temperature-dependent Hall measurements,[6] thus ruling out a pure compensation effect.

Recently, we have reported vibrational modes after hydrogen treatment for the chalcogen donors[16] that were independently confirmed by Rahbi *et al.*[17] The analysis of the frequency dependence on the donor species led to a model where the hydrogen atom binds in the antibonding position to one of the gallium atoms next to the donor atom with the gallium-hydrogen bond along a $\langle 111\rangle$ direction. This picture is in agreement with *ab initio* calculations performed by Chang[18] and Rahbi *et al.*[17] The complex has trigonal symmetry and the two absorption lines observed for each donor species are interpreted as a nondegenerate stretching mode and a lower-lying twofold degenerate bending mode.

The outline of this paper is as follows. After a description of the experimental details in the next section, experimental results are presented in Sec. III. Section IIIA will focus on local vibrational modes, temperature, and uniaxial stress effects, while Sec. IIIB presents the C-V and SIMS measurements. Results are discussed in Sec. IV and finally the conclusions are given in Sec. V.

II. EXPERIMENT

A. Samples

The samples used in this study consist of S- and Se-doped layers grown by metal-organic vapor phase epitaxy and Se-

and Te-doped layers grown by liquid phase epitaxy (LPE) on undoped semi-insulating GaAs substrates. The layer thicknesses varied between 2 and 10 μm with carrier concentrations from 2×10^{16} to 4×10^{18} cm^{-3} depending on the experimental technique the specimen was used for.

B. Setup

For passivation, the samples were exposed for 2–20 h to a remote hydrogen or deuterium dc plasma in a parallel plate system, with a plate voltage of $\sim$600 V. The samples were mounted on a heater block held at a temperature of 180–200 °C and placed 10 cm downstream from the plasma with a bias voltage of about -300 V, which fixed the bias current to 50 μA. The gas pressure was held at $\sim$1 mbar.

Infrared transmission was measured at normal incidence with a BOMEM DA3.01 Fourier transform spectrometer, equipped with a liquid-nitrogen-cooled MCT detector as well as a liquid-helium-cooled Si:B detector. To avoid mounting stress, the samples were free standing in the sample compartment of an exchange-gas cryostat, where the temperature was measured with a germanium or platinum resistor. Uniaxial stress measurements were performed in the same cryostat with the samples ($\approx2\times3\times8$ mm^3) mounted between the two pistons of a push rod system. The force was generated by a helium-gas-driven pneumatic cylinder and measured with a calibrated force sensor. All stress measurements were performed at 10 K. Polarized light was produced by putting a wire-grid polarizer with KRS-5 substrate in front of the cryostat.

For *C-V* depth profile measurements, Schottky diodes were fabricated by evaporating Au Schottky contacts of 0.6 mm in diameter after removal of 0.1–0.2 μm from the surface by a $H_2SO_4/H_2O_2/H_2O$ etch. Ohmic contacts were produced on the back side by scratching an In/Ga alloy. All annealing experiments are performed in the dark under nitrogen or helium atmosphere. Additionally, electrochemical *C-V* profiling was performed on the highly doped samples. Ohmic contacts were produced by alloying Sn contacts into the epitaxial layers. $(NH_4)_2C_4O_6$ diluted in NH_4OH solution was used as the electrolyte and the etching current was 0.3 mA/cm^2 with a contact size of 3.5 mm in diameter.

Secondary-ion-mass spectroscopy (SIMS) was performed on deuterated samples with a CAMECA IMS 4F using a Cs^+ primary beam. A Talystep surface profiler was used for the depth calibration and a hydrogen implanted sample (50 keV, 1×10^{15} cm^{-2}) for the calibration of the SIMS signal.

III. RESULTS

A. Localized vibrational modes

1. Vibrational frequencies, linewidth, and temperature effect

After hydrogen plasma treatment, two new absorption lines were found for each donor species, a stronger one around 780 cm^{-1} labeled *X*-H1 (*X*=S, Se, and Te) and a much weaker one *X*-H2 around 1500 cm^{-1} (cf. Ref. 16). Substituting hydrogen by deuterium shifts the spectral positions of the lines to lower frequencies by a factor close to $1/\sqrt{2}$ as expected for hydrogen LVM's, which are well described by a simple harmonic oscillator model. The precise ratios, together with the line positions, linewidths, and relative intensities at $T=10$ K are summarized in Table I. The integrated absorption after plasma treatment varies for unknown reasons, but the intensity ratio of *X*-H1 and *X*-H2 is constant to within experimental error, manifesting that they originate from the same complex. We attribute *X*-H1 to the bending mode of the bound hydrogen atom and *X*-H2 to the corresponding stretching mode. This assignment is confirmed by the uniaxial stress measurements presented later in this section. Assuming similar oscillator forces for both stretching mode and bending mode, the twofold degeneracy of *X*-H1 should lead to an intensity ratio close to 2, while experimentally a value of about 7 is found.

All observed lines exhibit a strong temperature dependence. Increasing the measurement temperature leads to a pronounced line broadening (Fig. 1) and a shift to lower frequencies (Fig. 2). The weaker higher-frequency lines *X*-H2 are observable only up to $T=50$ K, the stronger lower-frequency line S-H1 up to 240 K, and Te-H1 up to 110 K.

2. Effect of uniaxial stress

Uniaxial stress in the range from $\mathbf{F}=0-350$ MPa was applied along the three crystallographical directions [100],

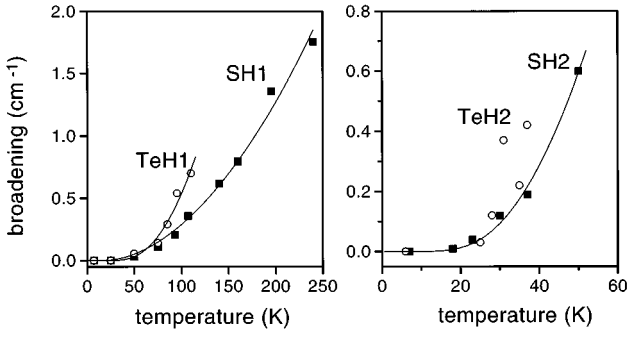

FIG. 1. Increase in linewidth with temperature of the S-H1/Te-H1 lines (left) and the S-H2/Te-H2 lines (right) (full width at half maximum). The linewidth at low temperature has been subtracted. The solid lines are obtained by the model of phonon scattering (cf. Table V).

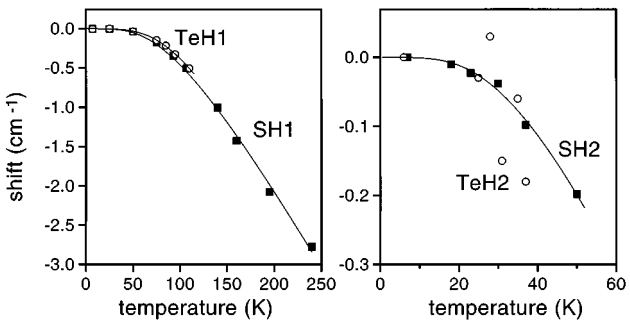

FIG. 2. Frequency shift with temperature of the S-H1/Te-H1 lines (left) and the S-H2/Te-H2 lines (right). The solid lines are obtained by the model of phonon scattering (cf. Table V).

TABLE I. Listing of LVM frequencies, their full width at half maximum (FWHM), relative integrated intensities, and r values ($r = \omega_{X-H}/\omega_{X-D}$) at $T = 10$ K.

Absorption line	Line position (10 K) (cm^{-1})	FWHM (10 K) (cm^{-1})	Relative intensity	r value (10 K)
S-H1	780.58	0.045	7.8	1.4035
S-H2	1512.30	0.071	1	1.3895
S-D1	556.1	0.3	7.6	
S-D2	1088.4	0.4	1	
Se-H1	777.95	0.08	7.3	1.4035
Se-H2	1507.46	0.08	1	1.3896
Se-D1	554.3	0.6	~20	
Se-D2	1084.8	0.7	1	
Te-H1	771.81	0.09	5.5	1.4033
Te-H2	1499.93	0.13	1	
Te-D1	550.0	0.6		
Te-D2		not detected		

[110], and [111] to hydrogenated Te-doped and Se-doped samples. Its effect on the two vibrational lines Te-H1 and Te-H2 was measured with the spectrometer light polarized parallel and perpendicular to the stress directions (Fig. 3). Figures 4 and 5 summarize the line splitting for the Te-H1/2 lines and Figs. 6 and 7 for the Se-H1/2 lines. In the latter case, due to the signal intensity, only unpolarized measurements were possible. For the [100] direction, it is found that Te-H1 splits into two components, one being fully polarized perpendicular to [100], the second being only partially polarized. For both the [110] and the [111] directions the line splits into three components with different polarization with respect to the stress direction. In contrast, the splitting of Te-H2 is much weaker. There is no line splitting for $\mathbf{F}\|[100]$, the line remains unpolarized and it is only displaced to higher frequencies. For $\mathbf{F}\|[110]$ a very weak splitting is observed. One of the two components is only visible with light polarized perpendicular to [110]. The Te-H2 line exhibits the largest stress effect for $\mathbf{F}\|[111]$. It splits into two components, one of which is fully polarized parallel to $\mathbf{F}$, the second being partially polarized. The relative intensities of the different components are given in the figures. In the case of the Se-H1/2 lines, the splitting pattern is very similar, except that not all of the components are resolved. This is a consequence of the larger linewidth of 0.6–0.7 cm^{-1} instead of 0.2 cm^{-1} for the Te-doped samples.

For none of the stress directions reorientation of the hydrogen atom could be observed. Maximum stress was applied to the sample at room temperature. After cooling the sample to liquid-helium temperature, stress was released and the absorption was measured with two different polarizations. To within experimental error, however, no anisotropy and as a consequence no reorientation of hydrogen complexes was detected.

B. Electrical passivation and reactivation

We have monitored hydrogen trapping and detrapping from tellurium and sulfur donors by capacitance-voltage profiling. By measuring the capacitance of a Schottky diode as a function of reverse bias voltage the depth-dependent free-carrier concentration can be calculated.

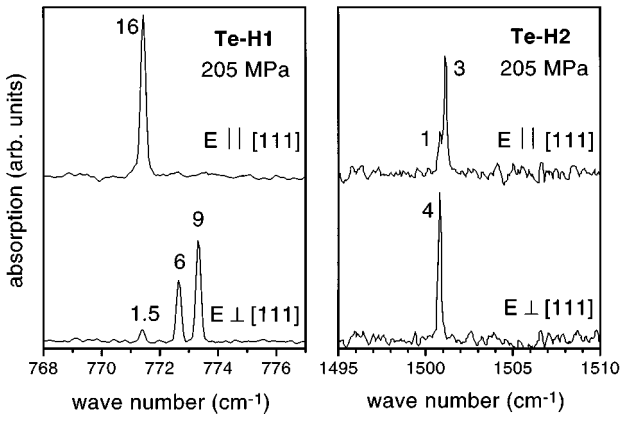

FIG. 3. Splitting of the absorption lines Te-H1 (left) and Te-H2 (right) for a uniaxial stress of 205 MPa parallel to the [111] direction. The upper spectra are measured with the light polarized parallel to the stress direction and the lower spectra with perpendicular polarization ($T = 10$ K). The numbers indicate the relative intensities of the various components.

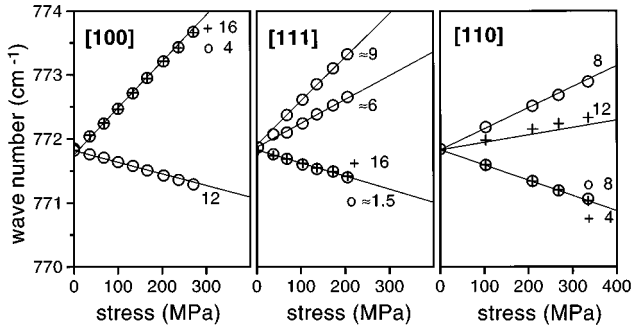

FIG. 4. Effect of uniaxial stress on the absorption line Te-H1 for stress directions parallel [100], [111], and [110], respectively, at $T = 10$ K. The straight lines are calculated using the fitted values of Table IV. The numbers indicate the relative intensities. Crosses are used for light polarized parallel to the stress direction and circles for the perpendicular polarization.

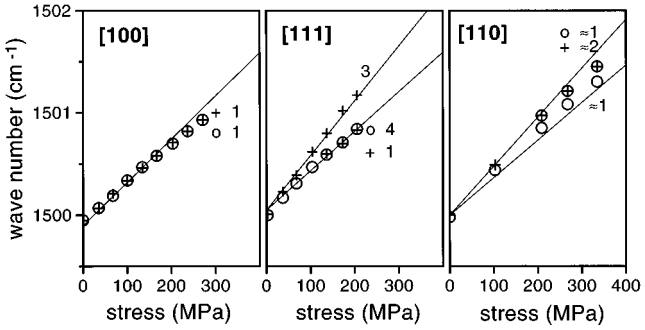

FIG. 5. Effect of uniaxial stress on the absorption line Te-H2 for stress directions parallel [100], [111], and [110], respectively, at $T=10$ K. The straight lines are calculated using the fitted values of Table IV. The numbers indicate the relative intensity. Crosses are used for light polarized parallel to the stress direction and circles for the perpendicular polarization.

For the Te-doped samples ($n=1.25\times10^{17}$ cm^{-3}), these measurements show a passivation, after 3 h of hydrogen plasma exposure at 200 °C, to a depth of about 0.4 μm. In this region the carrier concentration has decreased up to a factor of 10. For the annealing measurements, ~0.1 μm from the surface were removed before Schottky contacts were evaporated. Subsequently, the diode was aged for several hours at 160 °C without a bias voltage. For the following annealing steps a reverse bias of -2 V was applied while the sample was held in the dark. The result of a series of annealing steps is shown in Fig. 8. It shows a reactivation of the passivated donors in the near surface region and new passivation of donors deeper inside the layer. This can be interpreted as a thermal dissociation of the hydrogen complexes followed by a drift of the negatively charged hydrogen ions in the electric field of the diode. As the hydrogen accumulates in the deeper part of the sample, new complexes are formed. In order to determine the activation energy for the dissociation process, a monoexponential reactivation without retrapping of the released hydrogen is necessary (see below). For the Te-doped samples this regime was not reached even for the highest reverse voltages that could be applied (≈-5 V).

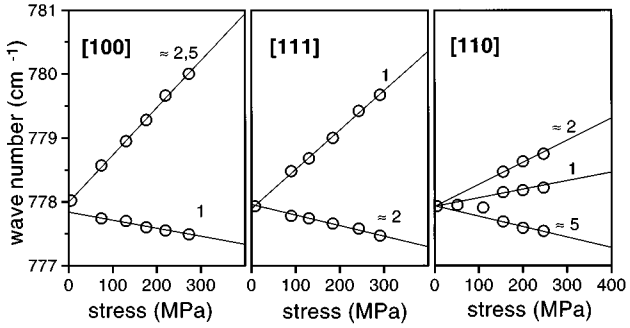

FIG. 6. Effect of uniaxial stress on the absorption line Se-H1 for stress directions parallel [100], [111], and [110], respectively (unpolarized light, $T=10$ K). The straight lines are calculated using the fitted values of Table IV. The numbers indicate the relative intensity.

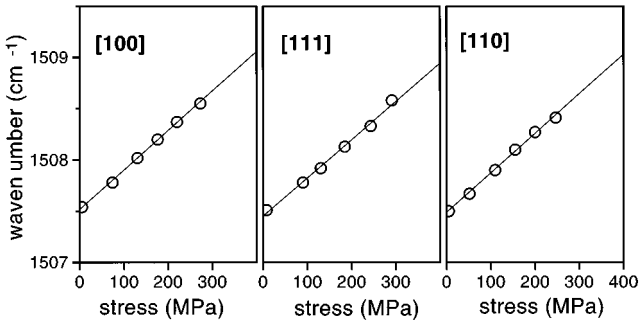

FIG. 7. Effect of uniaxial stress on the absorption line Se-H2 for stress directions parallel [100], [111], and [110], respectively (unpolarized light, $T=10$ K). The straight lines are calculated using the fitted values of Table IV. The numbers indicate the relative intensity.

Figure 9 shows similar measurements for S-doped layers ($n=1.8\times10^{16}$ cm^{-3}). In this case, the plateau region in the front part of the profile approaches the initial value exponentially with time. This reactivation was measured for various temperatures and is depicted in Fig. 10.

C. Depth profiles

In order to correlate the infrared signal and the electrically measureable passivation effect, infrared, *C-V*, and SIMS depth profiles were obtained on the *same* sample. Deuterium instead of hydrogen was used to increase the SIMS sensitivity.

The depth distribution of the absorbing S-D or Se-D complexes was determined by removing, step by step, material from the surface by a $H_2SO_4/H_2O_2/H_2O$ etch and by measuring simultaneously the absorption intensity at $T=10$ K. The final etching depth was obtained with a DEKTAK surface profiler and the intermediate values were interpolated from the etching time. Calculating the integrated absorption constant α_{int} (in cm^{-2}) of the S-D1/Se-D1 line, the complex concentration N as a function of depth can be estimated by the relation[19]

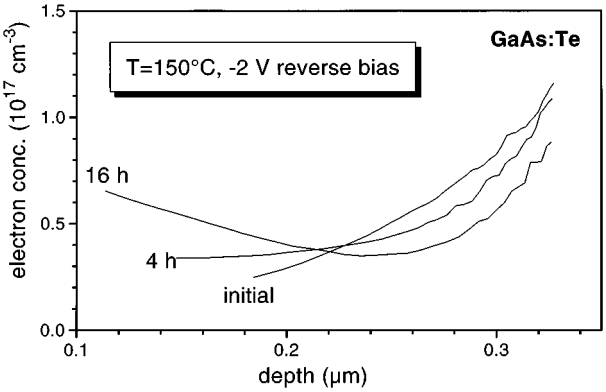

FIG. 8. Reactivation of passivated Te donors as a function of time in the space-charge region of a Schottky diode at $T=150$ °C with a reverse bias voltage of -2 V. The carrier concentration before hydrogenation was $n=1.3\times10^{17}$ cm^{-3}.

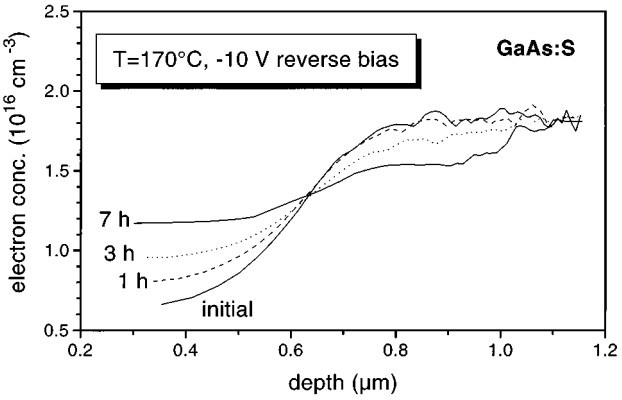

FIG. 9. Reactivation of passivated S donors as a function of time in the space-charge region of a Schottky diode at $T=170\,^{\circ}\mathrm{C}$ with a reverse bias voltage of -10 V. The carrier concentration before hydrogenation was $n=1.8\times10^{16}\ \mathrm{cm}^{-3}$.

$$N=\frac{2\,\varepsilon_0 n c^2 m}{\pi\eta^2}\,\alpha_{\mathrm{int}}, \tag{1}$$

where η is the apparent charge, n the refractive index, c the velocity of light, and m the vibrating mass. The formula assumes that the total absorption intensity goes into the S-D1/Se-D1 line. For hydrogen complexes in GaAs, η was found to be close to unity,[19] which was also assumed for our case.

In Fig. 11 the result is shown for a S-doped layer (~4 μm thick) after 18 h of plasma exposure at 200 °C. The SIMS measurement shows a higher deuterium concentration in the layer than in the undoped substrate. The difference corresponds well to the doping concentration of 2×10^{18} cm^{-3}. Furthermore, the infrared signal is detectable throughout the whole layer. However, using Eq. (1), the complex concentration is found to be a factor of 10 lower than the doping level.

Figure 12 shows the total deuterium concentration together with both the carrier profile (as measured by electrochemical C-V profiling) and the infrared active region for a second sample. For a depth $x>0.2$ μm, the deuterium concentration is below the doping concentration, while there is an excess hydrogen concentration close to the surface that coincides with a pronounced dip in the C-V profile. The

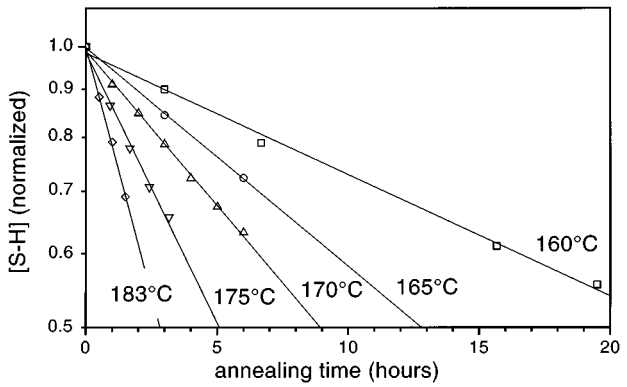

FIG. 10. Monoexponential dissociation of the S-H pairs with time as a function of annealing temperature. The annealing was performed in the dark with a reverse bias voltage of -10 V.

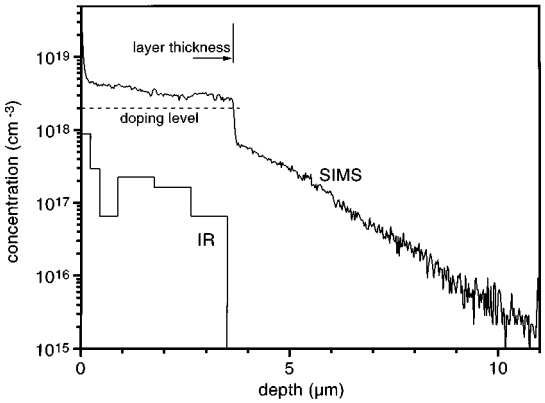

FIG. 11. Comparison of the total hydrogen content (SIMS) and the depth-dependent infrared absorption (IR) measured on the same sample (GaAs:S, $n=2\times10^{18}\ \mathrm{cm}^{-3}$). Deuterium was diffused into the sample for 18 h at 200 °C.

estimated concentration of infrared active complexes decreases with depth. After removal of 1.0 μm from the surface the signal intensity has decreased by about a factor of 10. Thus, taking into account the experimental error for all three kinds of measurements, this result suggests that the infrared active region coincides with the passivated part of the sample and that the observed infrared signal originates from the passivating complex.

IV. DISCUSSION

A. Vibrational frequencies at $T=10$ K

From Table I it is evident that there is a systematic dependence of the vibrational frequency on the mass of the donor atom. Increasing the donor mass leads to a decrease of the absorption frequency, indicating that the vibrational mode includes the donor atom. However, this line shift is very small compared to that found for group-IV donors or for hydrogen-acceptor complexes.[16] This indicates that the hydrogen atom in our case cannot be directly bound to the donor itself but to a host atom further away.

A similar case is known for the hydrogen passivated group-V donors P, As, and Sb in silicon.[1] Substituting the

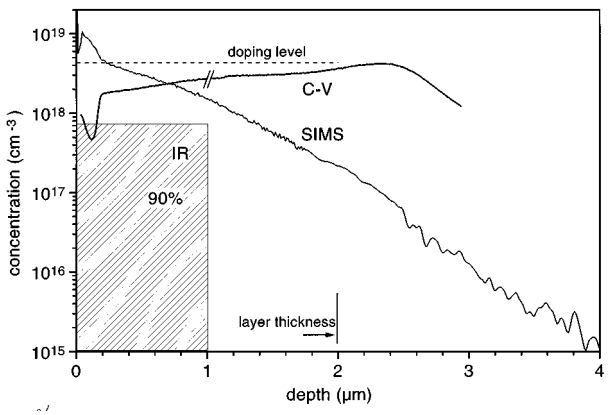

FIG. 12. Comparison of free carrier profile (C-V), total hydrogen content (SIMS), and infrared active region (IR) measured on the same sample (GaAs:Se, $n=4.5\times10^{18}\ \mathrm{cm}^{-3}$). Deuterium was diffused into the sample for 1.5 h at 200 °C.

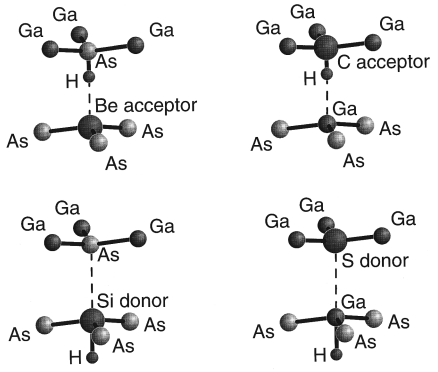

FIG. 13. Overview of acceptor and donor passivation by hydrogen in GaAs. Shown are the microscopic models established to explain passivation of group-II acceptors such as Be (Refs. 34 and 18), group-IV acceptors such as C (Ref. 35), group-IV donors such as Si (Refs. 34 and 18), and group-VI donors such as S (Ref. 18).

phosphorus donor (mass 31 a.u.) by antimony (mass 122 a.u.) shifts the hydrogen stretching LVM only by 7 cm^{-1} from 1555 cm^{-1} to 1562 cm^{-1}. For these complexes a model has been proposed, where the hydrogen atom binds in the so-called antibonding position to a neighboring silicon atom of the donor. Applying this model to our case suggests a hydrogen-gallium bond at the prolongation of the donor-gallium bond. The stretching frequency measured is in good agreement with the stretching frequency of 1550 cm^{-1} observed, for example, in the Ga-H radical.[20] As-H stretching modes usually are higher in frequency, such as in the case of arsine (2100 cm^{-1}).[21] On the other hand, however, one might expect the line to be split into a doublet, due to the two natural gallium isotopes ^{69}Ga (60.2%) and ^{71}Ga (39.8%). Experimentally, no splitting or line asymmetry was found. From this, an upper limit for the isotope shift of ~ 0.05 cm^{-1} can be given.

Finally, our picture is in perfect agreement with the model initially proposed by Chang.[18] It is based on *ab initio* pseudopotential calculations and predicts a trigonal complex with a strong hydrogen-gallium bond along a $\langle 111 \rangle$ direction. The gallium-donor bond is weakened and the gallium atom relaxes by 0.78 Å away from the donor to the hydrogen atom. Vibrational frequencies were calculated recently by Rahbi *et al.*[17] For the hydrogen (deuterium) complex they find a stretch frequency of 1592 cm^{-1} (1131 cm^{-1}) and a bending frequency of ~ 845 cm^{-1} (~ 600 cm^{-1}), assuming a harmonic potential. Figure 13 summarizes for comparison the microscopic models proposed to explain hydrogen passivation of the four types of donors and acceptors in GaAs.

B. Interpretation of uniaxial stress results

Without external perturbation, hydrogen complexes form on all equivalent lattice sites. For trigonal complexes (threefold axis of symmetry along $\langle 111 \rangle$) there are four possible equivalent orientations. In addition to this orientational degeneracy, the vibrational mode itself may be degenerated. Both kinds of degeneracy may be broken by applying uniaxial stress. The effect of this perturbation **F** on centers with various symmetries in cubic crystals has been calculated by Kaplyanskii[22] for centers with orientational degeneracy only and by Hughes and Runciman[23] for doubly degenerate tetragonal and trigonal centers. In Table II the calculated splitting of a nondegenerate trigonal center is summarized and Table III gives the corresponding expressions for a twofold degenerate mode of trigonal symmetry. The parameter $\mathscr{A}_1$ is the isotropic stress coefficient that describes the stress direction independent shift of the line pattern's ''center of mass.'' $\mathscr{A}_2$ induces a stress direction-dependent splitting of the lines caused by the center's orientational degeneracy. Finally, $\mathscr{B}$ and $\mathscr{C}$ describe the frequency splitting due to the removal of the degeneracy of the two-dimensional oscillator.

Our results for the Te-H1 line and the Te-H2 line (cf. Figs. 4 and 5) are well described by a trigonal center. As a consequence of the observed splitting pattern, Te-H1 is attributed to a twofold degenerate bending mode and Te-H2 to a nondegenerate stretching mode. Numerical fitting of the measured splitting Δ to the corresponding theoretical expressions leads to the pressure coefficients summarized in Table IV. The straight lines in Figs. 4 and 5 are calculated by using these values. The deviation from the experimental points is for most of the lines better than 10%. These results support the model presented in the preceding paragraph.

Since no reorientation of the hydrogen under stress has been observed, equivalent sites must be separated by a very high energy barrier or a long distance. In the case of Si_{As}-H complexes, where reorientation was observed,[24] the hydrogen atom is supposed to bind in the bond-centered position close to the acceptor atom, so that it can easily jump

TABLE II. Theoretical expressions for the stress-induced frequency splitting Δ of a nondegenerate vibrational mode of a trigonal center in a cubic crystal (Ref. 22). **F** is the applied stress, σ is its magnitude, **E** is the electric-field vector of the light, and $\mathscr{A}_1$, $\mathscr{A}_2$ are the stress coefficients.

Stress direction	Δ	Intensity $\mathbf{E}\parallel\mathbf{F}$	Intensity $\mathbf{E}\perp\mathbf{F}$
$\mathbf{F}\parallel[100]$	$\mathscr{A}_1\sigma$	1	1
$\mathbf{F}\parallel[111]$	$(\mathscr{A}_1+2\mathscr{A}_2)\sigma$	3	0
	$(\mathscr{A}_1-\frac{2}{3}\mathscr{A}_2)\sigma$	1	4
		Intensity $\mathbf{E}\parallel\mathbf{F}$	Intensity $\mathbf{E}\parallel[001]$
$\mathbf{F}\parallel[110]$	$(\mathscr{A}_1+\mathscr{A}_2)\sigma$	2	1
	$(\mathscr{A}_1-\mathscr{A}_2)\sigma$	0	1

TABLE III. Theoretical expressions for the stress-induced frequency splitting Δ of a doubly degenerate vibrational mode of a trigonal center in a cubic crystal (Ref. 23). **F** is the applied stress, σ is its magnitude, **E** is the electric-field vector of the light, and $\mathscr{A}_1$, $\mathscr{A}_2$, $\mathscr{B}$, and $\mathscr{C}$ are the stress coefficients.

Stress direction	Δ	Intensity $\mathbf{E}\parallel\mathbf{F}$	Intensity $\mathbf{E}\perp\mathbf{F}$
$\mathbf{F}\parallel[100]$	$(\mathscr{A}_1-2\mathscr{B})\sigma$	4	1
	$(\mathscr{A}_1+2\mathscr{B})\sigma$	0	3
$\mathbf{F}\parallel[111]$	$(\mathscr{A}_1+2\mathscr{A}_2)\sigma$	0	6
	$(\mathscr{A}_1-\frac{2}{3}\mathscr{A}_2-\frac{4}{3}\mathscr{C})\sigma$	16	1
	$(\mathscr{A}_1-\frac{2}{3}\mathscr{A}_2+\frac{4}{3}\mathscr{C})\sigma$	0	9
		Intensity $\mathbf{E}\parallel\mathbf{F}$	Intensity $\mathbf{E}\parallel[001]$
$\mathbf{F}\parallel[110]$	$(\mathscr{A}_1+\mathscr{A}_2+\mathscr{C}-\mathscr{B})\sigma$	0	0
	$(\mathscr{A}_1+\mathscr{A}_2-\mathscr{C}+\mathscr{B})\sigma$	1	2
	$(\mathscr{A}_1-\mathscr{A}_2+\mathscr{C}+\mathscr{B})\sigma$	0	2
	$(\mathscr{A}_1-\mathscr{A}_2-\mathscr{C}-\mathscr{B})\sigma$	3	0

from one acceptor-gallium bond to the neighboring one (cf. Fig. 13). The experimentally determined activation energy for Si_{As}-H is 0.26 eV, making reorientations possible above $T=85$ K. In our model, however, the hydrogen atom is sitting far away from the donor so that equivalent sites are separated by long distances and a direct jump seems to be unlikely.

C. Temperature effect

When considering the influence of temperature on vibrational transitions in semiconductors or ionic crystals, the observed effect can be divided into two major contributions: first, coupling of the vibrational motion under consideration (frequency ω) to other vibrations and, second, a volume effect that results from the thermal expansion $(\partial V/\partial T)_p$ of the lattice

$$\left(\frac{\partial\omega}{\partial T}\right)_p=\left(\frac{\partial\omega}{\partial T}\right)_V+\frac{\partial\omega}{\partial V}\left(\frac{\partial V}{\partial T}\right)_p=\left(\frac{\partial\omega}{\partial T}\right)_V-3\,B\alpha\frac{\partial\omega}{\partial p},$$

where $B=-V(\partial p/\partial V)_T$ is the bulk modulus, $\alpha=1/l\ dl/dT$ the linear thermal expansion coefficient of the host, and $\partial\omega/\partial p$ the directly measureable pressure dependence of the vibrational frequency.

Assuming for B and α the GaAs bulk values[25,26] and $\partial\omega/\partial p\approx 3$ cm^{-1}/GPa from the stress measurements, the contribution of the second term at $T=100$ K can be estimated to be

$$\Delta\omega\sim-3\,B\frac{\partial\omega}{\partial p}\int_0^{100\ \mathrm{K}}\alpha dT\sim-0.02\ \mathrm{cm}^{-1},\qquad(2)$$

TABLE IV. Listing of the measured pressure coefficients in cm^{-1}/GPa for the vibrational lines Se-H1/2 and Te-H1/2.

Line	$\mathscr{A}_1$	$\mathscr{A}_2$	$\mathscr{B}$	$\mathscr{C}$
Se-H1	3.0	0.67	−2.2	3.2
Se-H2	4.2	$-0.1\cdots+0.2$		
Te-H1	2.7	0.50	−2.3	3.3
Te-H2	4.2	0.56		

which is small compared to the observed temperature shifts. In addition, if the line shift were governed by the thermal lattice expansion, there should be a change in direction around $T=55$ K, where α changes its sign.[26]

In the following, we will thus concentrate on the first term that can be further divided into three different (homogenious) contributions. In addition, especially at low temperatures when these become small, inhomogenous broadening can be important, such as inhomogenous strain, internal electric fields, or isotope effects.

1. Phonon emission

Deexcitation by inelastic coupling to lattice phonons is only important for LVM's with a frequency not higher than two or three times the maximum lattice phonon frequency. In the case of GaAs, for LVM's higher than ~ 590 cm^{-1}, emission of three lattice phonons is necessary, which is a process of very low probability. It is in most of the cases negligible at higher temperatures when dephasing becomes important. The increase in linewidth $\Delta\Gamma$ is proportional to T^{n-1}, where n is the number of emitted phonons.[27].

2. Phonon scattering (''Raman dephasing'') (Refs. 28 and 27)

Interaction with lattice phonons without energy transfer, which means pure dephasing of the excited LVM state, results in a temperature-dependant Lorentzian linewidth and a positive or negative frequency shift with increasing temperature. The total interaction is given by the sum over all lattice phonon modes that are coupled to the LVM under consideration. Assuming an isotropic Debye model for the acoustic-phonon branches and no interaction with the optical phonons, McCumber and Sturge[28] found the temperature dependences

$$\Delta\omega(T)=A\left(\frac{T}{\Theta_c}\right)^4\int_0^{\Theta_c/T}\frac{x^3}{e^x-1}dx\propto\overline{E},\qquad(3)$$

$$\Delta\Gamma(T)=B\left(\frac{T}{\Theta_c}\right)^7\int_0^{\Theta_c/T}\frac{x^6e^x}{(e^x-1)^2}dx\qquad(4)$$

TABLE V. List of the parameters A, B, and Θ_c obtained by numerically fitting the measured temperature effect to Eqs. (3) and (4) (''phonon scattering model'').

	Line shift		Line broadening	
Line	A (cm^{-1})	Θ_c (K)	B (cm^{-1})	Θ_c (K)
S-H1	−24.0	366	3.5	146
S-H2	−6.8	155	55.6	162
Te-H1	−46.2	492	68.2	357
Te-H2				

for the lineposition ω, and the linewidth Γ, respectively. Here $k\Theta_c$ is an ''effective'' Debye cutoff energy that is somewhat smaller than the Debye energy $k\Theta_D$ and takes into account that not all of the acoustic branches interact with the LVM.[28] In this model, $\Delta\omega$ is proportional to the mean thermal energy E of the lattice. For temperatures high compared to Θ_c, these formulae exhibit the limiting behavior

$$\Delta\omega \propto T, \quad \Delta\Gamma \propto T^2$$

and for low temperatures $T \ll \Theta_c$ the model gives

$$\Delta\omega \propto T^4, \quad \Delta\Gamma \propto T^7.$$

3. Exchange coupling

Vibrational phase relaxation due to an anharmonic coupling of the LVM to *one particular* low-frequency mode has been studied by Persson and Ryberg[29] for the case of a stretch vibrational mode of molecules chemisorbed on a metal surface. The model consists of a high-frequency LVM of frequency ω that is perturbed by a vibrational mode of lower frequency ω_0, which has, due to some kind of damping, the width η. The nature of the low-frequency mode maybe either another mode of the molecule itself or one of the host crystal. The coupling between the two modes has the magnitude $\delta\omega$. In the general case, no analytical expressions can be given. This is only possible for two limiting cases.

(i) One is the weak-coupling limit $\delta\omega \ll \eta$:

$$\Delta\omega = \frac{\delta\omega}{e^{\hbar\omega_0/kT}-1}, \tag{5}$$

$$\Delta\Gamma = \frac{2\,\delta\omega^2}{\eta}\frac{e^{\hbar\omega_0/kT}}{(e^{\hbar\omega_0/kT}-1)^2}, \tag{6}$$

$$\frac{\Delta\Gamma}{(\Delta\Omega)^2} = \frac{2}{\eta}e^{\hbar\omega_0/kT}. \tag{7}$$

These expressions are valid for all temperatures. For higher temperatures $T \gg \omega_0$ the lineshift $\Delta\omega$ becomes linear with temperature and the linewidth Γ increases quadratically.

(ii) The other is the low-temperature limit $kT < \hbar\omega_0$:

$$\Delta\omega = \delta\omega\frac{\eta^2}{\delta\omega^2+\eta^2}e^{-\hbar\omega_0/kT}, \tag{8}$$

$$\Delta\Gamma = 2\,\eta\frac{\delta\omega^2}{\delta\omega^2+\eta^2}e^{-\hbar\omega_0/kT}. \tag{9}$$

These expressions are valid for all values of $\delta\omega$ and η. The characteristic result is the exponential temperature dependence, due to the freeze out of the perturbing mode ω_0.

In the case of hydrogen local vibrational modes in GaAs, which have high frequencies, only three of the broadening mechanisms presented above can contribute: frequency change due to thermal lattice expansion, elastic scattering of lattice phonons, and exchange coupling to one particular low-frequency mode. A distinction between these mechanisms is in general not an easy task, since the studied LVM's are only observable at low temperatures, which means only over a small temperature range. In addition, when investigating broadening at low temperatures, it has to be kept in mind that at these temperatures inhomogenous broadening might contribute too.

The observed temperature dependence can be simulated both with the phonon scattering model and with the exchange coupling model. The result of the first model is also given in Figs. 1 and 2 and the corresponding parameters are given in Table V. Although the values obtained are reasonable, there is a striking difference between the Θ_c values from the shifts and those obtained from the broadening. On the other hand, Fig. 14 shows the fitting to an exponential law, the one encountered for exchange coupling at low temperatures, and Table VI gives the values found for ω_0. There is reasonable agreement between the values from the line shift and broadening. Furthermore, these values indicate that the requirement $\hbar\omega_0 < kT$ is met for the measured temperature range, whereas the last column of the table shows that the weak-coupling case is not reached. In the case of the C_{As}-H stretching vibration in GaAs,[30] the same model could

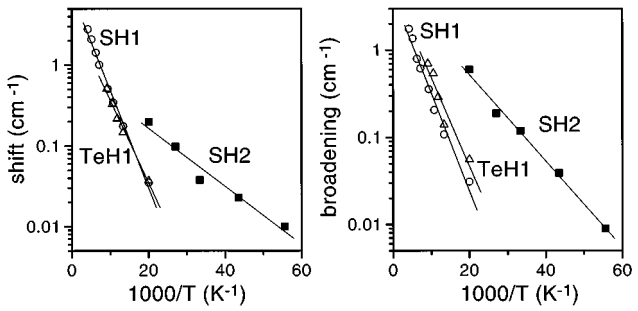

FIG. 14. Fitting of the temperature-induced frequency shift and broadening to an exponential law. The frequency values ω_0 deduced from the slopes $-\hbar\omega_0/kT$ are summarized in Table VI.

TABLE VI. List of the frequencies of the perturbing low-frequency modes ω_0 and the relative coupling strength $\delta\omega/\eta$ [cf. Eqs. (8) and (9)] (''exchange coupling model'').

Line	ω_0 (from shift)	ω_0 (from broadening)	$\delta\omega/\eta$
S-H1	193 ± 6 cm^{-1}	179 ± 10 cm^{-1}	~0.3
S-H2	57 ± 6 cm^{-1}	79 ± 4 cm^{-1}	~1.2
Te-H1	163 ± 10 cm^{-1}	162 ± 27 cm^{-1}	~0.7
Te-H2			

successfully be applied over a large temperature range (up to $T=300$ K) and the frequency found was $\omega_0=78$ cm^{-1}. It was assigned to transverse acoustic phonons at the X point of the Brillouin zone. A similar result was obtained when studying hydrogen passivated silicon donors in GaAs and AlAs.[31] The authors attribute the observed temperature effect to a dephasing by low-energy acoustic phonons. However, in all these cases no microscopic explanation for an efficient coupling of the LVM to these particular phonon vibrations could be given.

D. Dissociation kinetics of the S-H complex

Assuming a simple model for the formation and dissociation of donor-hydrogen pairs, the kinetics of S-H formation is described by the differential equation

$$\frac{\partial[\mathrm{SH}]}{\partial t}=\sigma[\mathrm{H}](n_0-[\mathrm{SH}])-\nu[\mathrm{SH}], \tag{10}$$

where [SH] is the local complex concentration, n_0 is the unpassivated shallow donor concentration, σ describes the cross section for hydrogen capture by the donor atom, and ν is the dissociation constant. If the dissociation of the complexes is purely thermally activated, then ν can be described by the temperature dependence

$$\nu(T)=\nu_0 e^{-E_{\mathrm{SH}}/kT}, \tag{11}$$

where ν_0 is the attempt frequency and E_{SH} the dissociation energy of the S-H complex. In the general case, there are two competing processes. (a) dissociation of complexes (hydrogen detrapping), whose rate is, in our model, purely determined by the sample temperature, and (b) complex formation (hydrogen trapping), which depends on both the concentration of unpassivated donors and the local free hydrogen concentration [H] (in the appropriate charge state). As a consequence, this latter process could be eliminated if it were possible to locally maintain a low free hydrogen concentration. In favorable cases this is possible by a reverse bias annealing technique, which was succesfully applied by Zundel and Weber[32] to the case of acceptors in silicon. Applying a reverse bias voltage to a hydrogen passivated Schottky diode during annealing leads to a fast drift of the detrapped charged hydrogen species in the high-electric-field region. Then the first term on the right-hand side of Eq. (10) becomes negligible compared to the dissociation term and the reactivation of the passivated donors follows a simple monoexponential law

$$[\mathrm{SH}]=[\mathrm{SH}]_{t=0}e^{-\nu t}. \tag{12}$$

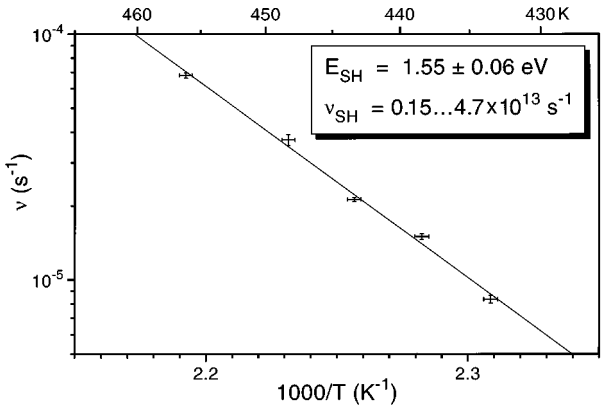

FIG. 15. Determination of the dissociation energy E_{SH} of the S-H complexes. ν is the dissociation rate at a given temperature and ν_{SH} the attempt frequency.

In Fig. 9, this is the case in the near surface region, where a plateau is formed. At 0.65 μm the carrier concentration remains constant, which signifies that here the trapping rate and the detrapping rate are equal. Finally, for depths greater than 0.65 μm hydrogen trapping dominates so that the carrier concentration decreases with annealing time. With the reverse bias voltage applied, the depth of the space-charge region was constant at 1.0 μm. The reactivation rate ν was measured for different temperatures (Fig. 10). According to Eq. (11), the activation energy for the dissociation process is obtained from an Arrhenius plot (Fig. 15). This leads to an energy of $E_{\mathrm{SH}}=1.55\pm0.06$ eV and an attempt frequency of $\nu_0\sim(0.15\text{–}4.7)\times10^{13}$ s^{-1}. Leitch, Prescha, and Weber[9] found for the Se-H pairs an energy value of $E_{\mathrm{SeH}}=1.52\pm0.05$ eV and an attempt frequency $\nu_0=2\times10^{13}$ s^{-1}. Thus, within experimental error, the energy values are identical for the S-H and the Se-H pairs. This fits the proposed model, where the hydrogen atom is bound to a gallium atom and not to the donor itself.

V. CONCLUSION

By application of Fourier transform infrared spectroscopy to hydrogen plasma treated S-, Se-, or Te-doped GaAs, a microscopic model for the donor passivation is developed. It is proposed that the hydrogen atom binds to a gallium nearest neighbor of the donor species in the antibonding position, so forming a trigonal, electrically inactive complex. Uniaxial stress measurements are in agreement with this picture: The lower frequency vibrational modes X-H1 (X=S, Se, and Te) are due to a twofold degenerate mode (hydrogen bending vibration) and the higher-lying absorption lines X-H2 correspond to a nondegenerate stretching mode of the hydrogen atom. This model explains the very weak frequency dependence on the donor mass and supports the calculations performed by Chang[18] and Rahbi *et al.*[17] However, no conclusive explanation can be given why the isotope effect caused by the two natural gallium isotopes is not seen. A strong gallium-arsenic bond is required so that the effective gallium mass becomes large and the isotope effect very small. However, there is actually no reliable way to quantitavely predict

from the proposed model how large the expected effect should be.

A strong temperature effect on the line positions and linewidths was observed. We have discussed several mechanisms that have been employed to explain the influence of temperature on LVM's in solids. An unambiguous distinction between the possible coupling mechanisms, however, is not possible. Applying the exchange coupling model, different perturbing modes in the acoustic-phonon range are found. They do not correspond to high symmetry points in the Brillouin zone and a microscopic picture of their coupling is unclear. The assumption of a coupling to *all* acoustic phonons can reproduce the experimental data as well. But in this case there is only poor agreement for the values obtained for the line broadening and the line shift. Since this model is rather empirical, no microscopic insight can be gained.

By measuring the dissociation energy of the S-H complex, we find a value of $E_{SH}=1.55\pm0.06$ eV with an attempt frequency of $\nu_{SH}\sim(0.15\text{–}4.7)\times10^{13}\ s^{-1}$, which are identical to the values previously found for the Se-H pairs ($E_{SeH}=1.52\pm0.05$ eV, $\nu_{SeH}=2\times10^{13}\ s^{-1}$).[9]

Although, from experiment and theory, much is known now about the microscopic mechanism of shallow dopant passivation by hydrogen, there are still many open questions concerning the hydrogen diffusion process. It is found that the correlation between hydrogen penetration and dopant passivation often is poor. One important factor is the hydrogenation technique employed[33] since it determines, for example, the rate of hydrogen incorporation into the material. Inside the bulk, the kinetics of hydrogen diffusion is crucially influenced by its charge state because hydrogen drift and trapping by impurities is governed by the electric field. There are still many open questions concerning the possible charge states and under which forms hydrogen can be present in the GaAs lattice. Finally, our results show that in general only a part of the hydrogen atoms present in the crystal give rise to a detectable infrared or electrical signal. Most of it is present in another, yet unknown form.

ACKNOWLEDGMENTS

We wish to thank A. W. R. Leitch and J. R. Botha for the growth of sulfur-doped samples, as well as S. Zehender and E. Bauser for the LPE samples and C. Geng and D. Ottenwälder for the MOCVD samples, and we appreciate the technical assistance of E. Lux. Finally, we are grateful to Professor H.-J. Queisser for his continued interest and support and acknowledge the technical assistance of H.-W. Krause and W. Heinz.

[1] S. J. Pearton, J. W. Corbett, and M. Stavola, *Hydrogen in Crystalline Semiconductors* (Springer, Berlin, 1992).
[2] S. J. Pearton, Mater. Sci. Forum **148-149**, 393 (1994).
[3] R. Darwich, B. Pajot, B. Rose, D. Robein, B. Theys, R. Rahbi, C. Porte, and F. Gendron, Phys. Rev. B **48**, 17 776 (1993).
[4] B. Clerjaud, D. Côte, and W. S. Hahn, Mater. Sci. Forum **148-149**, 281 (1994).
[5] J. Chevallier, A. Jalil, R. Azoulay, and A. Mircea, Mater. Sci. Forum **10-12**, 591 (1986).
[6] B. Theys, B. Machayekhi, J. Chevallier, K. Somogyi, K. Zahraman, P. Gibart, and M. Miloche, J. Appl. Phys. **77**, 3186 (1995).
[7] M. Stavola, Mater. Sci. Forum, **148-149**, 251 (1994).
[8] A. J. Tavendale, S. J. Pearton, A. A. Williams, and D. Alexiev, Appl. Phys. Lett. **56**, 1457 (1990).
[9] A. W. R. Leitch, Th. Prescha, and J. Weber, Phys. Rev. B **44**, 1375 (1991).
[10] B. Machayekhi, R. Rahbi, B. Theys, M. Miloche, and J. Chevallier, Mater. Sci. Forum **143-147**, 951 (1994).
[11] R. Rahbi, D. Mathiot, J. Chevallier, C. Grattepain, and M. Razeghi, Physica B **170**, 135 (1991).
[12] B. Clerjaud, F. Gendron, M. Krause, and W. Ulrici, Phys. Rev. Lett. **65**, 1800 (1990).
[13] G. Roos, N. M. Johnson, C. Herring, and J. Walker, Mater. Sci. Forum **143-147**, 933 (1994).
[14] L. Pavesi and P. Giannozzi, Phys. Rev. B **46**, 4621 (1992).
[15] S. J. Pearton, W. C. Dautremont-Smith, J. Chevallier, C. W. Tu, and K. D. Cummings, J. Appl. Phys. **59**, 2821 (1986).
[16] J. Vetterhöffer, J. H. Svensson, J. Weber, A. W. R. Leitch, and J. R. Botha, Phys. Rev. B **50**, 2708 (1994).
[17] R. Rahbi, B. Theys, R. Jones, B. Pajot, S. Öberg, K. Somogyi, M. L. Fille, and J. Chevallier, Solid State Commun. **91**, 187 (1994).
[18] K. J. Chang, Solid State Commun. **78**, 273 (1991).
[19] B. Clerjaud and D. Côte, J. Phys. Condens. Matter **4**, 9919 (1992).
[20] K. P. Huber and G. Herzberg, *Molecular Spectra and Molecular Structure IV Constants of Diatomic Molecules* (Van Nostrand Reinhold, New York, 1979).
[21] K. Nakamoto, *Infrared Spectra of Inorganic and Coordination Compounds* (Wiley, New York, 1970).
[22] A. A. Kaplyanskii, Opt. Spektrosk. **16**, 606 (1964) [Opt. Spectrosc. (USSR) **16**, 329 (1964)].
[23] A. E. Hughes and W. A. Runciman, Proc. Phys. Soc. London **90**, 827 (1967).
[24] D. M. Kozuch, M. Stavola, S. J. Spector, S. J. Pearton, and J. Lopata, Phys. Rev. B **48**, 8751 (1993).
[25] J. S. Blakemore, J. Appl. Phys. **53**, R128 (1982).
[26] S. I. Novikova, Fiz. Tverd. Tela (Leningrad) **3**, 178 (1961) [Sov. Phys. Solid State **3**, 129 (1961)].
[27] R. J. Elliott, W. Hayes, G. D. Jones, H. F. MacDonald, and C. T. Sennett, Proc. R. Soc. London Ser. A **289**, 1 (1965).
[28] D. E. McCumber and M. D. Sturge, J. Appl. Phys. **34**, 1682 (1963).
[29] B. N. J. Persson and R. Ryberg, Phys. Rev. B **32**, 3586 (1985).
[30] B. Clerjaud, D. Côte, F. Gendron, W.-S. Hahn, M. Krause, C. Porte, and W. Ulrici, Mater. Sci. Forum **83-87**, 563 (1992).
[31] E. Tuncel and H. Sigg, Phys. Rev. B **48**, 5225 (1993).
[32] T. Zundel and J. Weber, Phys. Rev. B **39**, 13 549 (1989).
[33] W. C. Dautremont-Smith, in *Defects in Electronic Materials*, edited by M. Stavola, S. J. Pearton, and G. Davies, MRS Symposia Proceedings No. 104 (Materials Research Society, Pittsburgh, 1988), p. 313.
[34] P. R. Briddon and R. Jones, Phys. Rev. Lett. **64**, 2535 (1990).
[35] B. Clerjaud, F. Gendron, M. Krause, and W. Ulrici, Phys. Rev. Lett. **65**, 1800 (1990).